Aerosol Spectroscopy of Dihydroxyacetone: Gas Phase and Nanoparticles

Ruth Signorell*

Institut für Physikalische Chemie, Universität Göttingen, Tammannstrasse 6, D-37077 Göttingen, Germany

David Luckhaus

Laboratorium für Physikalische Chemie, ETH Zürich, Universitätstrasse 22, CH-8092 Zürich, Switzerland

Received: August 8, 2001; In Final Form: December 18, 2001

Dihydroxyacetone aerosols with particle diameters around 50 nm were produced in an electrospray at ambient temperature and pressure. The vibrational spectra of the aerosols between 800 and 4000 cm^{-1} were recorded with a Fourier transform infrared spectrometer. Depending on the experimental conditions, an appreciable amount of gas-phase 1,3-dihydroxy-2-propanone appeared in the infrared spectra of the particulate phase. In contrast to the gas phase, the particulate phase was found to consist of the chemically bound dimer 2,5-dihydroxymethyl-2,5-dihydroxy-1,4-dioxane. Temperature-dependent gas-phase spectra of dihydroxyacetone monomer between 310 and 440 K reveal interesting torsional dynamics, which are analyzed with the help of a detailed four-dimensional model. Experimental spectra of the nanoparticles were simulated using a Kramers−Heisenberg dielectric function. The comparison with ab initio calculations of the free molecule and small clusters leads to a first microscopic picture of the intermolecular interactions in the condensed phase.

1. Introduction

The combination of spectroscopy and theoretical modeling offers an elegant approach to the process of molecular aggregation on a microscopic level.[1,2] With the noted ability of the OH group to act both as proton donor and as proton acceptor, sugars provide ideal models for studying molecular aggregation processes in hydrogen-bonded systems[3]. 1,3-Dihydroxy-2-propanone (dihydroxyacetone) is the simplest ketose, and like other sugars, it forms multiple hydrogen-bonds. In the gas phase, there is a maximum of two intramolecular hydrogen bonds, which stabilize this molecule in a bicyclic conformation[4] (section 4). With the carbonyl group as a competing acceptor of hydrogen bonds, one expects to observe a complex interplay between intra- and intermolecular hydrogen bonding in the formation of condensed phases. As infrared spectra of the crystalline bulk phase[5] have revealed, the aggregation is accompanied by a change of the chemical nature of the molecular subunit—the formation of the chemically bound dimer 2,5-dihydroxymethyl-2,5-dihydroxy-1,4-dioxane. This dimerization is the intermolecular analogue of the formation of cyclic hemiacetals or hemiketals in larger sugar molecules, such as glucose. The intermolecular interactions and the chemical nature of the molecular subunit (monomer/dimer) determine the formation dynamics and the structure of the solid phase, in particular, whether it is amorphous or crystalline. Its properties therefore make dihydroxyacetone an interesting model system to follow the interplay of conformational change, isomerization, and dimerization from the isolated molecule in the gas phase to solid nanoparticles and eventually to the bulk material.

The present work combines Fourier transform infrared (FTIR) spectroscopic investigations of small dihydroxyacetone particles and its gas phase in aerosols with theoretical predictions of the vibrational dynamics. With typical diameters around 50 nm, the particles investigated here fall in the class of nanoparticles.[6] Temperature-dependent gas-phase spectra and detailed dynamical simulations lead to a first microscopic picture of the torsional dynamics in the monomer (section 4). The infrared spectra of nanometer-sized dihydroxyacetone particles are discussed in section 5.1. In recent years, similar molecular mesoscopic systems held together by multiple hydrogen bonds or dispersion interactions have received some attention (refs 7−18 and references therein). Most of these studies are devoted to volatile molecular substances for which an independent detailed characterization of the particle-size distributions is not always possible. The combination of electrospray generation with an accurate size characterization, as it is used in the present study, is an important step forward toward the generation of narrow, well-characterized particle distributions. These form the basis for subsequent quantitative evaluations including the determination of optical constants from particle extinction spectra (refs 19 and 20 and references therein). Optical constants enable the proper spectroscopic characterization of condensed matter. Their knowledge (and that of particle spectra in general) is therefore of crucial importance in atmospheric research and in the investigation of interstellar dust (see, for instance, refs 9 and 21). The determination of optical constants in turn leads to the fundamental question to what extent data deduced from particle spectra are comparable to those determined from bulk material and vice versa. For molecular systems, this problem is closely related to the structure of the molecular subunits involved and to the nature of the intermolecular forces that hold them together. The determination of optical constants from the dihydroxyacetone particle spectra is outlined in section 5.2. We assume a damped harmonic oscillator model (Lorentz model[22,23]) to describe the interaction of the condensed phase with the electromagnetic field. The results are compared with those obtained from a direct inversion of the spectra exploiting the Kramers−Kronig relation for the refractive index.[22,23] The spectroscopic parameters extracted from the Lorentz model can

* To whom correspondence should be addressed. Fax: +49 551 393117. E-mail: rsignor@gwdg.de.

10.1021/jp0130968 CCC: $22.00
Published on Web 04/18/2002

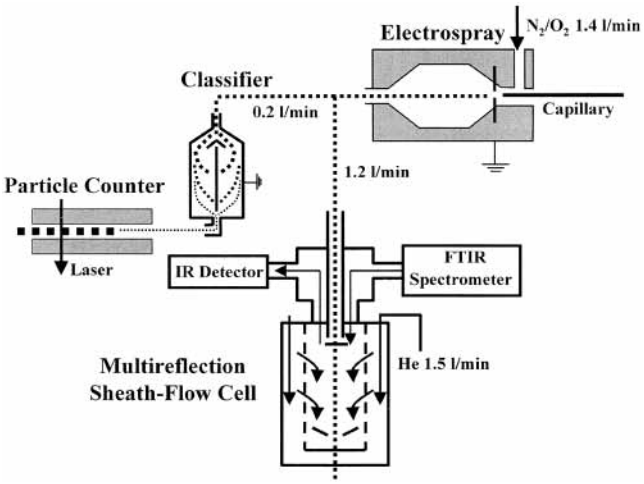

Figure 1. Schematic view of the experimental setup used to generate and measure the aerosols.

be compared with ab initio calculations of isolated molecules and clusters (section 5.3). This comparison with molecular properties in the gas phase allows identification of the effects that are characteristic of the condensed phase. We conclude by discussing the implications of the results for the mechanism of aggregation and for the structure of the solid phase of this prototype system of hydrogen-bonded networks.

2. Experiment

The gas-phase infrared spectra of 1,3-dihydroxy-2-propanone ($C_3H_6O_3$; Fluka puriss.; available as dihydroxyacetone dimer) were measured in a heatable 3 m long single-path glass cell. The electrical heating was arranged in three zones along the cell in which the temperatures were regulated with the help of three NiCr−Ni thermocouples. In addition, the two KBr windows at the ends of the cell, the outlet to the rotary vane pump, and the sample tube were heated separately. Again, the temperatures were measured with NiCr−Ni thermocouples. In the range between 293 and 443 K, the temperature along the cell was stable within 3 K.

The gas-phase infrared spectra were recorded with a resolution of 2 cm^{-1} using a Bruker Vector 22 FTIR spectrometer, a mid-infrared Globar light source, a KBr beam splitter, and a DTGS (deuterated triglycine sulfate) or InSb (indium antimonide) detector. The measurement time typically amounted to 2 min. The spectra were apodized with a Norton−Beer medium function.

The experimental setup for the measurements of the aerosol spectra is displayed schematically in Figure 1. Additional details concerning the different components are outlined in refs 3,16, and 24−27. The aerosol was generated with an electrospray aerosol generator (EAG; TSI 3480) from an aqueous buffer solution of dihydroxyacetone (ammonium acetate and ammonium hydroxide in H_2O puriss. (Fluka)). By varying the concentration of dihydroxyacetone, the diameter of the nanoparticles could be varied between 20 and 90 nm. The particles left the EAG supported in synthetic air (1.4 L/min, Messer 5.0, 20.5% O_2 in N_2). To measure the number size distribution of the generated particles simultaneously with the infrared spectra, 0.2 L/min of the aerosol flow was guided through the scanning mobility particle sizer (SMPS). The SMPS consists of an electrostatic classifier (TSI 3080N) and a condensation particle counter (TSI 3022A). The classifier determines the particle diameters, d_j, for the different size intervals, j. Each decade of particle size is divided into 64 equidistant logarithmic intervals. The particle counter then measures the particle number concentration, N_j, in each interval j.

The remaining 1.2 L/min of the aerosol flow entered the multireflection sheath-flow cell[16,26,27] for the spectroscopic investigation. The cell consists of two concentric cylinders. The carrier gas is introduced into the gap between the two, enters the inner cylinder through a large number of small holes, and is pumped off at the bottom. This creates a smooth sheath flow for samples injected coaxially at the top of the inner cylinder. The cell was operated at room temperature with a sheath flow of 1.5 L of He per minute. The sheath flow served to guide the dihydroxyacetone aerosol through the flow tube and to minimize contaminations of the mirrors. The cell was equipped with White optics. In the present investigation, the optical path length amounted to $h = 16$ m. This value represents an upper limit to the effective absorption path length because the aerosol stream may not completely fill the optical path. In previous studies on CO_2 and N_2O nanoparticles using a similar experimental setup,[18] gas pulses of CO_2 were introduced into the sheath flow. The extinction observed for CO_2 corresponded to 50% of the value expected for the amount actually introduced into the cell (with optical constants taken from the literature). For the present experiments, this leads to a very cautious lower bound of the effective optical path length of 8 m. With the continuous gas inlet used here, the deviation from the nominal optical path length of 16 m is presumably much smaller. The infrared spectra were recorded at a resolution of 3 cm^{-1} with a Bruker IFS 66v/S spectrometer equipped with a Globar light source, a KBr beam splitter, and a MCT detector. The spectra were apodized with a Blackman−Harris function.

To compare the nanoparticle spectra with bulk data, we have recorded FTIR spectra of crystalline dihydroxyacetone in KBr pellets, of thin layers of solid dihydroxyacetone, and of aqueous dihydroxyacetone solutions. The thin layers were prepared by rapid evaporation of a saturated methanol/dihydroxyacetone solution on a NaCl window or by deposition of gas-phase dihydroxyacetone on a KBr window. Aqueous solutions were measured between AgCl windows. FTIR spectra were recorded in ambient air at room temperature with the Bruker Vector 22 spectrometer.

3. Calculations

3.1. Ab Initio Calculations and 4D-Torsional Dynamics. A recent ab initio study[4] has identified four stable conformers of 1,3-dihydroxy-2-propanone. A comparison of density functional theory (DFT) with second order Moller−Plesset (MP2) perturbation theory using the 6-31G** basis set revealed overall close agreement of the B3LYP functional with MP2 theory. This conclusion, however, was reached solely on the basis of equilibrium geometries and electronic energies. Vibrational effects were completely neglected. They should be particularly important in dihydroxyacetone in which the conformational dynamics are largely determined by its intramolecular hydrogen-bonding characteristics. To obtain a more complete structural characterization and in particular to relate it to the experimentally observable spectroscopic properties, we have determined optimized geometries, electronic energies, and harmonic fundamental transition wavenumbers and intensities for basis sets up to triple-ζ quality including polarization functions. The results for different stable conformations of the monomer obtained with the B3LYP functional were compared with MP2 calculations to check the reliability of the method for the description of the spectroscopic properties and of the conformational dynamics of the monomer as well as the dimer. All calculations were

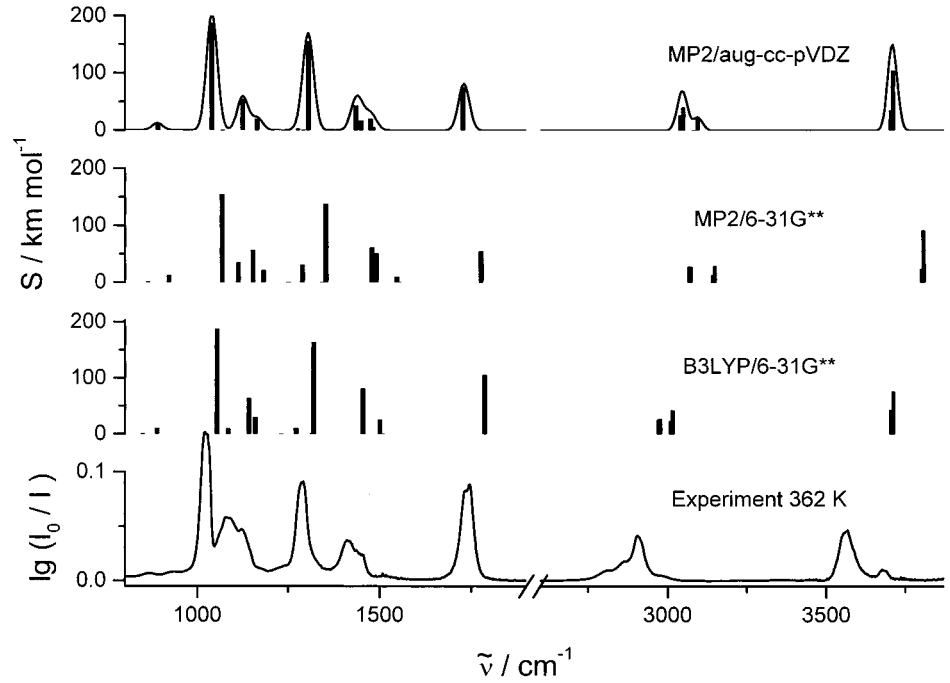

Figure 2. The gas-phase infrared absorption spectrum of dihydroxyacetone. A comparison of different levels of ab initio theory with experiment (bottom trace) is shown. The stick spectra are calculated in harmonic approximation. For better comparison with the experimental spectrum, the top trace was convoluted with a Gaussian band shape of 50 cm^{-1} fwhm.

performed with the Gaussian program package.[28] The DFT calculations employed integration grids of 50 radial shells with 194 angular points each, pruned to about 7500 grid points per atom. The MP2 calculations included only valence orbitals (frozen core approximation).

Figure 2 compares the experimental gas-phase IR spectrum with some of the calculated vibrational fundamental spectra. The agreement is already very good even for the modest B3LYP/6-31G** level of theory. Increasing the basis size or the level of theory produces only small shifts of the transition wavenumbers, as exemplified in Figure 2 by the results of MP2/aug-cc-pVDZ calculations. At that level of theory, the spectrum of the isolated molecule is almost perfectly reproduced considering that unscaled ab initio harmonic wavenumbers are compared with experimental anharmonic transitions. Typical anharmonicities will shift CH and OH stretching fundamentals to lower wavenumbers by about 100 cm^{-1} in agreement with experiment. There are only two minor deviations left: the weak absorption on the low wavenumber side of the CH stretching fundamentals, due to the characteristic CH-stretch−bend Fermi resonance, and the weak absorption about 100 cm^{-1} above the OH stretching fundamental, which will be discussed below. Neither of them is due to deficiencies of the treatment of the electronic structure. On the contrary, even the overall intensity distribution is very well described already at the B3LYP/6-31G** level. A more detailed discussion of the ab initio calculations will be deferred to a separate publication. Here, we only note that B3LYP/6-31G** provides a realistic description of the gas-phase spectra of monomeric dihydroxyactone. This includes its hydrogen-bonding characteristics justifying the use of the B3LYP/6-31G** approach for further investigating the conformational stability and dynamics of this system.

To derive a potential hypersurface for the conformational dynamics in the four torsional angles around the C−C (χ) and C−O (τ) single bonds (see Figure 3), one-dimensional (1D) and two-dimensional (2D) minimum energy paths and surfaces were explored under various constraints in these angles. It turned out that the torsional motion induces only minor changes in the bond

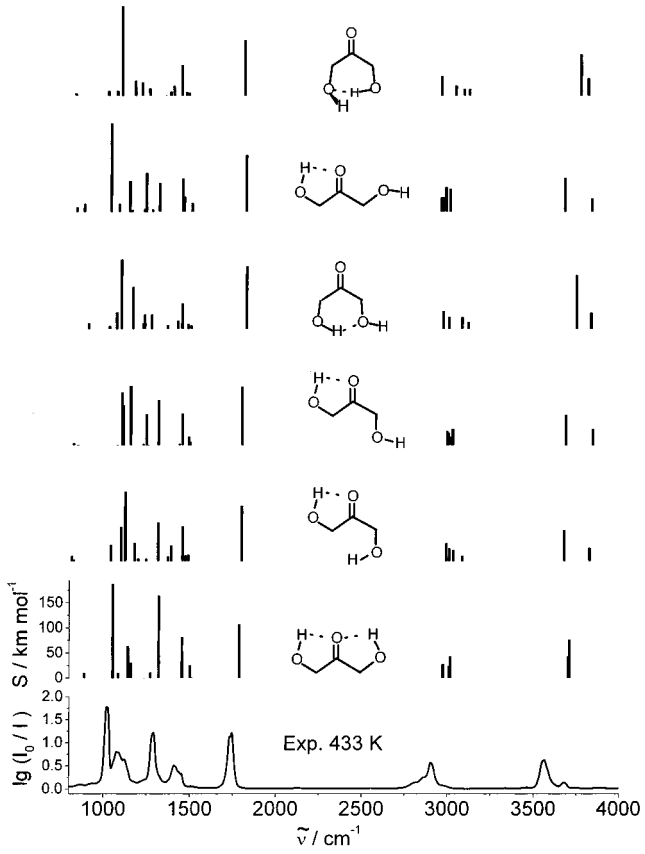

Figure 3. Theoretical stick spectra of the different conformers of dihydroxyacetone calculated on the B3LYP/6-31G** level. The spectra are arranged from bottom to top in order of increasing energy (including zero-point correction) of the six corresponding local minima of the conformational space (see Table 2). The bottom trace is the experimental gas-phase spectrum.

lengths and bond angles. Table 1 collects their mean values and standard deviations for the 2D minimum energy surface

TABLE 1: Average Geometry of Dihydroxyacetone on the B3LYP/6-31G Minimum Energy Surface as a Function of Torsional Angles $\chi_1 = \chi_2$ and $\tau_1 = \tau_2$[a]**

r, Å		β, deg		δ, deg	
r(C=O)	1.2132(31)	β(O=C−C)	120.77(161)	δ(H−C−C=O)	122.01(301)
r(C−C)	1.5335(51)	β(C−C−O)	112.17(367)	δ(C−CO−C)	180.00(6)
r(C−O)	1.4185(80)	β(C−O−H)	108.61(107)		
r(O−H)	0.9647(17)	β(C−C−H)	108.02(174)		
r(C−H)	1.0991(39)				

[a] r is bond length, β is bond angle, and δ is dihedral angle. Standard deviations from mean values are given in parentheses in terms of the last digits.

constrained to pairwise equal torsional angles. We have calculated a 4D torsional potential with bond lengths and angles frozen at these values. The potential was computed using the iterative successively averaged spline interpolation (SASI,[29]) from a total of about 10 000 single-point calculations using the B3LYP density functional with the 6-31G** basis set. The 4D torsional eigenvalue problem was solved using the generalized Z-matrix discrete variable representation together with the adiabatic truncation and contraction technique described in ref 30.

To account for the anharmonicity of the torsional dynamics the vibrational partition function, Q_{vib}, of a given conformer was calculated according to

$$Q_{\mathrm{vib}} = \sum_i \exp(-E_i/(k_{\mathrm{B}}T)) \prod_{k=11}^{3N} (1 - \exp\{-\omega'_k hc/(k_{\mathrm{B}}T)\})^{-1} \quad (1)$$

The ω'_k parameters are the nonzero harmonic wavenumbers of the projected force field, F', from which the four torsional degrees of freedom have been explicitly removed:

$$F' = (1 - \sum_k \delta_k \delta_k^{\mathrm{T}}) F (1 - \sum_k \delta_k \delta_k^{\mathrm{T}}) \quad (2)$$

The δ_k parameters are normalized mass-weighted Cartesian displacement vectors corresponding to the infinitesimal translations, rotations, and torsions ($\chi_{1,2}$, $\tau_{1,2}$). T indicates the transpose. In eq 1, E_i are the eigenvalues of 4D torsional problems, which have been confined to the coordinate ranges corresponding to different conformers (see section 4).

For the dimer of dihydroxyacetone (2,5-dihydroxymethyl-2,5-dihydroxy-1,4-dioxane), we have calculated optimized geometries, electronic energies, harmonic fundamental transition wavenumbers, and intensities for the three different isomers. These differ in the positions of the OH and CH_2OH groups with respect to the dioxane ring in its most stable chair conformation (i.e., equatorial or axial). The calculations were performed on the B3LYP/6-31G** level. Calculations using larger basis sets (6-311G** and 6-311++G**) for one of the isomers produced only insignificant changes in the geometries and in the vibrational spectrum. In particular, we note here that the inclusion of diffuse basis functions does not significantly affect the calculated spectrum despite the presence of multiple hydrogen bonds.

3.2. Determination of Optical Constants. The frequency-dependent complex refractive index, $n + ik$, of dihydroxyacetone was determined directly from the experimental extinction spectrum of the nanoparticles between 800 and 4000 cm^{-1} by following two alternative approaches, the Lorentz model fit and the Kramers−Kronig inversion. Both proceed via the complex refractive index to characterize the optical properties of the particulate phase. We employed Mie theory for spherical particles[23] to calculate the observed extinction spectrum. The refractive index of the surrounding medium (essentially He buffer gas) was set to unity.

The frequency-dependent extinction cross sections, C_j, are calculated separately for each value of the particle diameter, d_j. The total calculated absorbance, A_{calc}, is then obtained by summing over all different diameters using the experimental particle size distribution:

$$A_{\mathrm{calc}} = h \sum_j N_j C_j \quad (3)$$

where h is the optical path length and N_j is the number density of aerosol particles with size d_j determined independently as described in section 2. As further discussed in section 5.2, the effective optical absorption path length, h, only enters as a constant scaling factor into the determination of the optical constants.

The Mie theory gives the solutions for the scattering and absorption of light by spherical particles. The assumption of a spherical shape should be an adequate model because we are dealing with amorphous dihydroxyacetone particles (see section 5.1). Equation 3 also neglects multiple scattering. For this approximation to be valid, the scattering contribution, $C_{\mathrm{sca},j}$, to the extinction cross section should be small (see, for example, ref 23), that is,

$$h \sum N_j C_{\mathrm{sca},j} \ll 1 \quad (4)$$

With the refractive index determined here for dihydroxyacetone, we obtain $h\sum N_j C_{\mathrm{sca},j} \leq 10^{-5}$, therefore, justifying the neglect of contributions from multiple scattering in the present study. For these small particles, the Mie scattering calculations could be carried out in the so-called "Rayleigh" limit without any significant loss of accuracy (see ref 23, page 135).

In the first approach to determine the complex refractive index of the nanoparticles, we assume a model function for the (complex, frequency-dependent) dielectric function, ϵ, of the dihydroxyacetone particles. The empirical parameters of this function are determined from a nonlinear least-squares fit of the calculated extinction, A_{calc} (eq 3), to the experimental aerosol spectra. In this study, we have used the so-called Lorentz model, which describes the optical properties of the solid by a collection of isotropic damped harmonic oscillators coupled to the electromagnetic field of the light by their effective charge. Solution of the classical equations of motion leads to the Kramers−Heisenberg dielectric function:[22,23]

$$\epsilon = \epsilon_1 + i\epsilon_2 = \epsilon_{\mathrm{e}} + \sum_s \left(\frac{\tilde{\nu}_{\mathrm{s}}^2 f_{\mathrm{s}}}{\tilde{\nu}_{\mathrm{s}}^2 - \tilde{\nu}^2 - i\gamma_s \tilde{\nu}} \right) \quad (5)$$

The dielectric function is directly related to the complex index of refraction (n,k):

$$n = \sqrt{\frac{\sqrt{\epsilon_1^2 + \epsilon_2^2} + \epsilon_1}{2}} \qquad k = \sqrt{\frac{\sqrt{\epsilon_1^2 + \epsilon_2^2} - \epsilon_1}{2}} \quad (6)$$

The parameter ϵ_{e} is the value of the dielectric function at frequencies that are high compared with the vibrational excitations considered (but low compared with electronic excitations, which are neglected here). Equation 5 sums over all oscillators in the spectral region of interest. They are characterized by their

resonance wavenumber, $\tilde{\nu}_s$, their reduced oscillator strength, f_s, and a width, γ_s, resulting from the damping of the oscillator.

To the extent that a Lorentz oscillator can be compared to a molecular oscillator (e.g., a molecular normal mode), $\tilde{\nu}_s^2 f_s$ is proportional to the absorbance, $\int A(\tilde{\nu})\, \mathrm{d}\nu$, integrated over the corresponding absorption band (also termed integrated intensity). Equation 5, however, neglects any local field correction, that is, it assumes that each oscillator experiences the external electric field, which is not necessarily a good approximation in the condensed phase. An approximate local field correction for isotropic media leads to a formally identical expression,[31] but with shifted resonance wavenumbers and modified effective reduced oscillator strengths. For the relatively small values of the reduced oscillator strengths found in the vibrational spectrum of dihydroxyacetone, the wavenumber shifts can be neglected. The modification of the reduced oscillator strengths significantly changes their absolute values, thus affecting their interpretation in terms of molecular transition moments.[31] The relative values, however, remain approximately unchanged by the local field correction. In the present study, the comparison of theoretically (ab initio) calculated intensities with the corresponding empirical Lorentz model parameters, $\tilde{\nu}_s^2 f_s$, will therefore be restricted to relative values.

In the second approach, we exploit the Kramers−Kronig relation between the real (n) and the imaginary (k) part of the complex refractive index.[22,23] The optical constants can thus be derived from the experimental extinction spectrum without assuming any particular model. In its so-called subtractive form, the Kramers−Kronig relation[32,33,34] is given by the following equation:

$$n(\tilde{\nu}') = n(\tilde{\nu}_\mathrm{r}) + \frac{1}{\pi}\int_{\tilde{\nu}_\mathrm{min}}^{\tilde{\nu}_\mathrm{max}} \left(\frac{k(\tilde{\nu})}{\tilde{\nu} + \tilde{\nu}'} - \frac{k(\tilde{\nu})}{\tilde{\nu} + \tilde{\nu}_\mathrm{r}} + \frac{k(\tilde{\nu})}{\tilde{\nu} - \tilde{\nu}'} - \frac{k(\tilde{\nu})}{\tilde{\nu} - \tilde{\nu}_\mathrm{r}} \right) \mathrm{d}\tilde{\nu} \quad (7)$$

Equation 7 requires the knowledge of the real index of refraction at some reference point, $\tilde{\nu}_\mathrm{r}$. Although in principle arbitrary, it is best chosen to lie within the spectral region of interest. When one starts with some guess for the real part, n, of the refractive index, its imaginary part k is adjusted (by bisection) so that the Mie scattering calculation reproduces the experimentally measured extinction separately for each value of the wavenumber $\tilde{\nu}$. Equation 7 is then applied to $k(\tilde{\nu})$ to produce an improved guess for $n(\tilde{\nu})$. The Cauchy principal value of the integral in eq 7 was calculated on a grid as described in ref 34 with the difference, however, that $k(\tilde{\nu})$ was expanded to fourth order around the singularity at $\tilde{\nu} = \tilde{\nu}'$. The whole procedure is repeated until convergence is reached. Because the reference value, $n(\tilde{\nu}_\mathrm{r})$, of the real index of refraction cannot be determined through this procedure, it enters as the only free parameter. Here, it was set to the value obtained from the Lorentz model fit at 2600 cm^{-1}, where the experimentally measured extinction vanishes. Otherwise, this second approach to the determination of optical constants constitutes an inversion of the experimental spectrum rather than a fit.

4. Gas Phase

The often small number density of nanoparticles in aerosols necessitates the use of sensitve spectroscopic detection techniques. Under such conditions, even a low vapor pressure will produce detectable amounts of gas-phase molecules, which will contribute to the observed extinction spectra. Moreover, in the form of nanoparticles even substances generally regarded as nonvolatile may evaporate to an appreciable amount due to the increase of the vapor pressure with decreasing radius of curvature (Kelvin effect). In aerosol spectroscopy, it is therefore essential to know gas-phase spectra to distinguish the vapor from the particulate solid phase. IR spectra of the trioses, dihydroxyacetone and glyceraldehyde, have been known both in the solid state and in solution for 30 years,[5,35] but no gas-phase spectra have been measured prior to this work. In the following, we present the first gas-phase IR spectra of dihydroxyacetone, the more stable of the two trioses. Beyond the more technical aspect just mentioned, the spectroscopy of the isolated monomer is interesting in its own right. In comparison with detailed theoretical models, it allows us to learn about the characteristics of the intramolecular hydrogen-bond dynamics. Some of the results will be transferable to the dimer and the condensed phase for which the complexity limits the applicability of detailed theoretical models. Figure 3 compares the IR spectrum of dihydroxyacetone vapor recorded at 433 K with the harmonic fundamental transitions calculated ab initio for different conformers of dihydroxyacetone. The conformational landscape is determined by the hydrogen-bonding characteristics of the two hydroxyl groups and the carbonyl group. At the B3LYP/6-31G** level of theory, we find a total of six local minima, schematically depicted in Figure 3. The stable conformations are connected by torsional motion around the C−C and C−O single bonds leaving the molecular frame largely unchanged. The electronic energies and relative energies including harmonic zero-point corrections are listed in Table 2 together with corresponding MP2 results. We also note that the equilibrium geometries are very similar for the two ab initio approaches as are in fact the calculated harmonic fundamental spectra. The doubly H-bridged all-cis conformer represents the energetically most favorable arrangement in agreement with previous ab initio studies.[4] To within systematic deviations expected for the harmonic approximation, the calculated fundamental transitions agree perfectly with the experimental gas-phase spectrum. We have further validated our approach by comparing the B3LYP/6-31G** calculations for the most stable conformer with results obtained with larger basis sets using DFT as well as MP2 theory (see section 3). The good agreement justifies using the same approach to model the spectroscopic and structural properties of the dimer (sections 5.2 and 5.3), which in turn provide the foundation for analyzing aerosol and other condensed-phase spectra.

In addition to the validation of the DFT approach for the dimer, the spectroscopic investigation of the monomer in the gas phase allows quantification of the energetics ruling the

TABLE 2: Electronic Energies (E) and Vibrational Zero-Point Energies (ZPE) of Different Conformers of Dihydroxyacetone with Respect to the Most Stable Conformer, cccc

	B3LYP/6-31G**		MP2/6-31G**	
	ΔE (hc cm^{-1})	ΔZPE (hc cm^{-1})	ΔE (hc cm^{-1})	ΔZPE (hc cm^{-1})
cccc	0	0	0	0
tccc	764	+49	597	+12
tctc	840	−43	625	−72
tttc	1582	+166	1012	+141
cctc	1980	−55	1835	−76
ttcc	1939	+207	1605	+167

[a] The electronic energy of the conformer cccc amounts to −343.584 00 E_h (B3LYP) and −342.625 19 E_h (MP2), and its ZPE is 20 688 cm^{-1} (B3LYP) and 21 225 cm^{-1} (MP2). The four letter labels refer to the approximate values of (χ_1, χ_2, τ_1, τ_2). "c" corresponds to ∼0° (cis) and "t" to ∼180° (trans) (see also Figure 3).

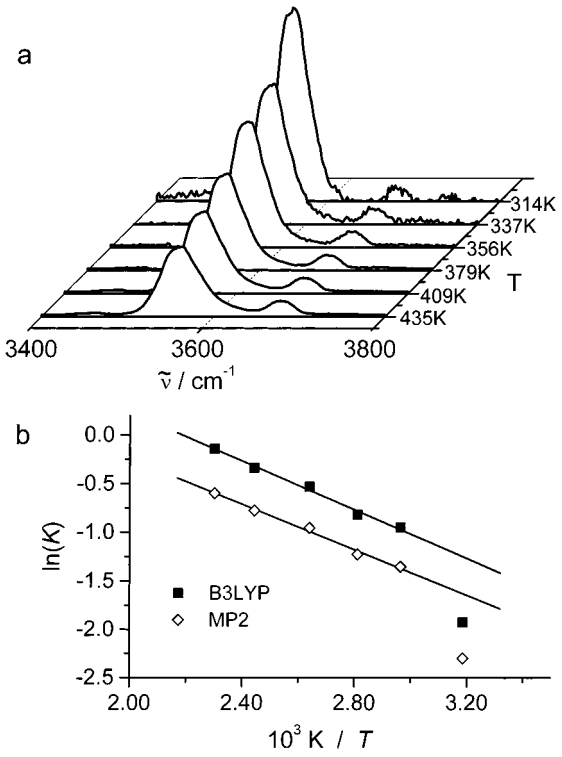

Figure 4. Temperature dependence of the gas-phase absorption spectrum of dihydroxyacetone. Panel a shows the OH-stretching region of the experimental gas-phase spectrum as a function of temperature. The absorbance traces are scaled to equal absorbance at 3640 cm^{-1}. Panel b shows the Van't Hoff plot of the ratio K of open and bound conformers. K was derived from experimental intensity ratios using different theoretical band strengths ((■) B3LYP; (◇) MP2; both 6-31G**, see text).

conformational dynamics of dihydoxyacetone. Shifted by 120 cm^{-1} to higher wavenumbers from the OH stretching fundamental, the gas phase spectra distinctly show a second, weaker absorption. With increasing temperature, this band becomes more and more pronounced compared with the lower main band. This is shown in Figure 4a by the absorption spectra in the range of the OH stretching fundamentals recorded at temperatures between 314 and 435 K. The spectra are normalized to the blue-shifted weaker absorption band to illustrate the effect more clearly. From the comparison of ab initio spectra in Figure 3, it is clear that this band must be assigned to the free OH group of less-stable open conformers of dihydroxyactone. With the transition moments calculated ab initio, we can derive an experimental value for the reaction energy for the formation of open conformers. This quantity essentially represents the strength of the C═O···H−O hydrogen bond. For this purpose, we assign the weak band near 3680 cm^{-1} to the second most stable conformer (index 2). The strong band near 3560 cm^{-1} therefore has contributions both from the most stable conformer (index 1) and from conformer 2. Thus, the ratio, K, of populations 2 to 1 is given by

$$K = r\sigma_{I,1}/(\sigma_{II,2} - r\sigma_{I,2}) \qquad (8)$$

The σ parameters are the relative band strengths calculated ab initio for the lower (bound, I) and higher (free, II) OH stretching fundamental transitions of the different conformers; r is the ratio of the integrated band strengths of the two bands (II/I) observed experimentally. We chose the range for integration from 3490 to 3720 cm^{-1} with the separation between the two bands set to the position of the absorption minimum at 3650 cm^{-1}. The

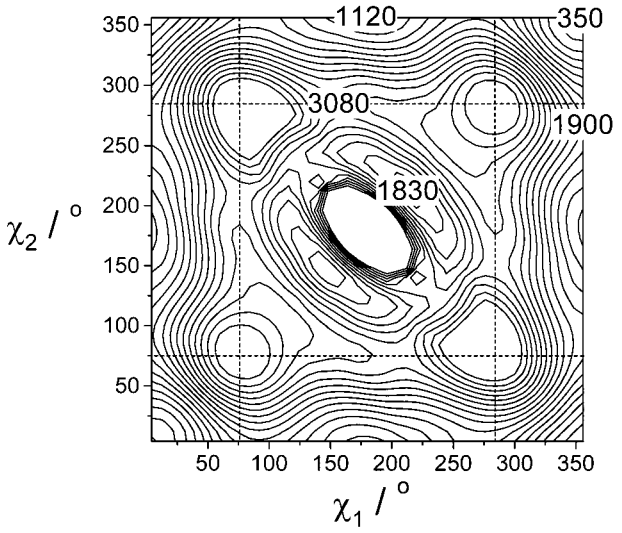

Figure 5. Two-dimensional adiabatic potential surface in the CO torsional angles ($4° \le \chi \le 356°$) for the vibrational ground state of the OH torsions (τ). Contours represent equipotential lines separated by 200 cm^{-1}. Labels indicate approximate potential values for the three different types of minima and the saddle points connecting them. The dashed lines separate the coordinate ranges, which define the three distinguishable conformers.

logarithmic van't Hoff plot of K vs the inverse temperature is shown in Figure 4b for two different choices of ab initio transition moments. Both data sets lie on straight lines, slightly shifted but parallel to each other. Consequently, one obtains virtually the same reaction energy whether one uses B3LYP or MP2 transition moments. The final value of 840 cm^{-1} (∼10 kJ/mol) results from least-squares fits to the data between 337 and 435 K. The value at 314 K was excluded because the exceedingly weak absorption signal makes the band strength of the band at 3680 cm^{-1} very uncertain. From the difference between the B3LYP and MP2 results, we estimate an uncertainty of 10% or 1 kJ/mol.

The experimental value of 840 cm^{-1} is to be compared with ab initio results of 814 cm^{-1} and 640 cm^{-1} using B3LYP and MP2 theory, respectively. These were derived from the temperature dependence of the Boltzmann populations of the conformers including rotational (rigid rotor) and vibrational (harmonic oscillator) contributions. The results are dominated by the electronic energy differences between the conformers with the B3LYP value distinctly closer to experiment than the MP2 value. This picture changes completely once the anharmonicity of the large amplitude torsional motion is properly taken into account. For this purpose, we have constructed a potential energy hypersurface in the four torsional angles as described in section 3 and solved the resulting 4D vibrational problem using the Z-matrix DVR technique described in ref 30. We defer a more detailed discussion of the conformational dynamics of dihydroxyacetone to a separate publication. It turns out that the motion in the CO and OH torsion angles occurs on distinctly separate time scales. As a result, the slow CO torsion can be viewed as taking place on effective 2D potential surfaces for each OH torsional state. This adiabatic separation of slow CO torsion and fast OH torsion is completely analogous to the Born−Oppenheimer separation of nuclear and electronic motion. Figure 5 shows the 2D CO torsional potential for the OH torsional ground state. One important consequence of the adiabaticity of the torsional dynamics is the reduction of distinct conformers from six to three due to the fast OH torsional averaging on time scales of 1 ps. The dotted line in Figure 5

separates the coordinate ranges assigned to the three conformers. They are referred to as cis−cis, cis−trans, and trans−trans according to the position of the OH groups relative to the carbonyl group at the minima of the adiabatic potential. Thus, the second, weak OH stretching band near 3680 cm^{-1} can be assigned to the cis−trans conformer. We have calculated torsional partition functions for each conformer by solving the 4D vibrational Schrödinger equation with appropriate boundary conditions, that is, the eigenfunctions were constrained to vanish outside the respective coordinate ranges. From the eigenvalues together with the projected harmonic wavenumbers for the remaining vibrational degrees of freedom, one obtains partition functions that now include the torsional anharmonicities (eq 1). The resulting reaction energy of 540 cm^{-1} (6.5 kJ/mol) for the formation of the cis−trans conformer is markedly different from the value obtained with the torsion treated in the harmonic approximation. Anharmonic contributions thus are comparable in size to the overall H-bond energy! The seemingly perfect agreement between experiment and DFT evidently results from a fortuitous cancellation of errors. The deviation of about 300 cm^{-1} (4 kJ/mol) between the anharmonic B3LYP value and the experimental value is more in line with expectations at this level of theory. Within this limit, however, B3LYP theory apparently provides a qualitatively and at least semiquantitatively correct description of the conformational dynamics in dihydroxyacetone. Building on this conclusion drawn for the monomer from careful checks against experiment and higher levels of theory, we take the same DFT approach to model the dimer, keeping in mind the importance of anharmonic contributions on the order of several kJ/mol to the relative stability of different conformers.

5. Nanoparticles

5.1. Experimental Spectra. The top trace in Figure 6a shows the extinction spectrum of dihydroxyacetone aerosol between 800 and 4000 cm^{-1}. The corresponding particle number size distribution is depicted in Figure 6b. The most frequent diameter (mode value) lies around 69 nm. The total particle number concentration and the total particle volume (assuming spherical particles) amount to 7.3×10^6 cm^{-3} and 1.8×10^{12} nm^3/cm^3, respectively. To investigate the influence of particle size, we have measured infrared spectra of particles with diameters between about 20 and 90 nm. Apart from the trivial scaling of the absorbance with the total particle volume, there is no unusual size dependence of band intensities or band positions in the infrared spectra of particles in this size range. This observation is in line with the results found for sucrose nanoparticles of similar size.[3] With increasing residence time of the aerosol in the flow cell, additional features appear in the spectra as depicted in the second trace (from top) of Figure 6a. Similar effects are observed upon a slight increase of the ambient temperature. On the basis of our gas phase study discussed in the previous section, we have been able to assign these additional features unambiguously to monomeric dihydroxyacetone in the gas phase. For illustration, Figure 6a also compares the difference of the two aerosol spectra (third trace from top) with a gas-phase spectrum recorded at 321 K (bottom trace). It was not possible to detect any gas phase over solid dihydroxyacetone samples in a stationary 3 m glass cell. Therefore, the observation of monomeric gas-phase dihydroxyacetone in the aerosol spectra indicates an increased evaporation of the nanoparticles compared with solid bulk material.

The increase of the gas-phase contribution with residence time indicates nonequilibrium between particles and vapor in the aerosol. Typically, we have found larger vapor-phase contributions for particle size distributions with higher concentrations of very small particles (20 nm and below). Such very small particles form a secondary maximum in the particle size distribution even for distributions with much larger mean diameters. Remnants of such a secondary maximum can be seen in Figure 6b. The original amount of these very small particles immediately after the aerosol formation in the electrospray can depend very sensitively on the experimental conditions. They may well be much larger than the remnants that can be seen as a secondary maximum in Figure 6b. The larger vapor pressure of such very small particles due to the Kelvin effect could explain the increased evaporation. For a droplet of diameter d, the Kelvin effect increases the vapor pressure by a factor of $\exp(4\gamma M/(\rho RTd))$ compared with the bulk (γ, M, and ρ are surface tension, molecular weight, and density, respectively). Because the surface tension is not known for dihydroxyacetone, we cannot provide a quantitative estimate. Assuming the same surface tension as for water ($\gamma = 0.072$ N/m) would lead to a 4-fold increase of the vapor pressure for a particle diameter of 10 nm compared with the bulk ($M = 180$ g/mol, $\rho \approx 1.5$ g/cm^3). This explanation is supported by measurements with mean particle diameters down to 20 nm, which invariably show larger gas-phase contributions.

The observation of monomeric dihydroxyacetone in the gas phase is the more remarkable because the aerosol particles themselves do not obviously contain any monomer. This is clearly demonstrated by the absence of the characteristic carbonyl stretch band around 1740 cm^{-1} in the top trace of Figure 6a. The most plausible assumption would be that the aerosol

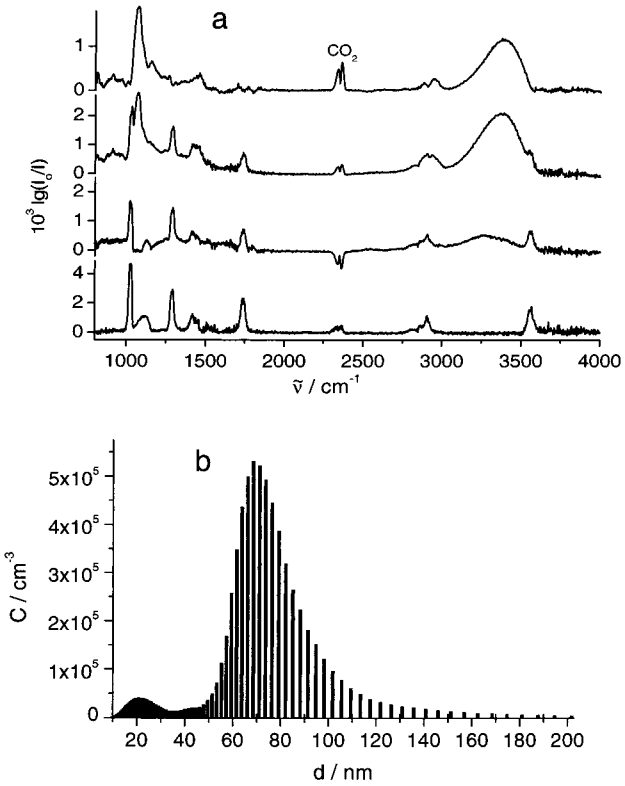

Figure 6. FTIR spectra of dihydroxyacetone (a): (top trace) FTIR spectrum of dihydroxyacetone nanoparticles; (second trace from top) aerosol spectrum, which shows the particle spectrum superimposed by the gas-phase spectrum due to evaporation of the particles (most frequent diameter = 73 nm); (third trace from top) difference of the two top traces scaled to equal maximum absorbance; (bottom trace) gas-phase spectrum recorded at 313 K. Panel b shows the measured particle number size distribution corresponding to the top trace of panel a (most frequent diameter = 69 nm).

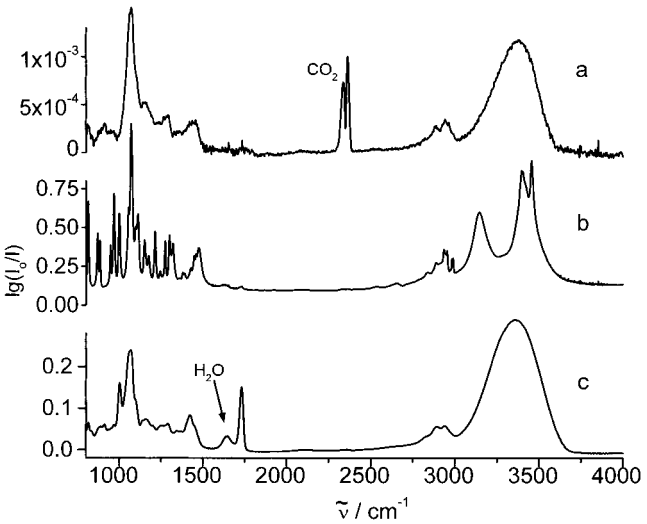

Figure 7. FTIR spectra of (a) dihydroxyacetone aerosol (most frequent particle diameter = 55 nm), (b) crystalline dihydroxyacetone in KBr, and (c) thin layer of dihydroxyacetone on a NaCl window obtained by evaporation of a solution in methanol.

particles have the same composition as the solid bulk. Figure 7 compares the aerosol spectrum (panel a) with that obtained from a KBr pellet of a crystalline sample (panel b). As mentioned in the Introduction, the crystalline bulk phase is known to consist of the chemically bound dimer, 2,5-dihydroxymethyl-2,5-dihydroxy-1,4-dioxane.[5] This intermolecular hemiketal depicted in Figure 10a,b has no carbonyl group left. Consequently, there is no carbonyl stretch band in the infrared spectrum of the KBr pellet (Figure 7b) in agreement with the aerosol spectrum (Figure 7a). Although the KBr pellet spectrum shows more fine structure than the aerosol particle spectrum, the overall intensity distribution is very similar. Therefore, the nanoparticles in aerosols formed from aqueous solutions in the electrospray most likely have the same molecular composition as the crystalline bulk phase, that is, 2,5-dihydroxymethyl-2,5-dihydroxy-1,4-dioxane. The much broader absorption features, however, are a clear indication of the amorphous nature of these particles.

The exact composition of the aqueous solution of dihydroxyacetone is not known, but it must contain significant amounts of dihydroxyacetone monomer. This is obvious from the prominent carbonyl band that we have found in the spectra of the aqueous solutions from which the particles were formed in the electrospray (see also refs 5 and 35−38). This implies that the particle generation in the electrospray is accompanied by a chemical reaction. The formation of solid dihydroxyacetone through condensation directly from the gas phase or through evaporation of methanolic solutions invariably leaves the dimerization incomplete. This is evident from the carbonyl band observed in the infrared spectrum of a thin film of dihydroxyacetone produced by evaporation of a solution in methanol shown in Figure 7c. Films resulting from condensation of dihydroxyacetone vapor lead to very similar results.

In line with previous semiquantitative kinetic studies,[5,35,37,38] the dimerization must be very efficiently catalyzed in the protic environment of an aqueous solution. It must be complete on the time scale of the aerosol formation, within seconds. By the same token, it is clear that the aerosol particles formed in the electrospray must dry very quickly and completely, as significant contents of water would immediately produce monomeric dihydroxyacetone. The remarkably fast and complete drying of the aerosol particles formed in the electrospray is consistent with the results of a previous study of sucrose aerosols.[3]

5.2. Optical Constants. From the observations in the previous section, we conclude that the dihydroxyacetone nanoparticles are formed in an amorphous solid state with dimeric (2,5-dihydroxymethyl-2,5-dihydroxy-1,4-dioxane) molecular subunits. For an amorphous state, one expects that the extinction spectrum of small particles in the mid-infrared region is mainly determined by the absorption features of the molecular subunit. Because of intermolecular interactions, however, the absorption bands of the aerosol can be shifted, broadened, and different in intensity compared with the gas-phase spectrum of the molecular subunit. The analysis of these effects can provide information about the microscopic structure of the particles. In this study, we have thus found indications of hydrogen bonds between the molecular subunits producing some degree of local order even in the amorphous state of dihydroxyacetone particles. A full understanding of such effects requires a detailed microscopic picture of the structure of the particles. As a first step in this direction, important insights can be obtained from the analysis of the spectroscopic properties in terms of simple models.

The optical properties of the condensed phase are described by the dielectric function or, equivalently, the optical constants. To analyze and interpret these quantities, we exploit the Kramers−Heisenberg form of the dielectric function[22] used to fit the experimental aerosol spectra. This approach does not only provide a useful compact parametrization of experimental optical constants. Its foundation on the Lorentz model allows us to go even further and relate the optical properties of the solid particles to the properties of the molecular subunits from which they are built. As discussed in section 3.2, this model describes the solid as a collection of damped harmonic oscillators coupled to the electromagnetic field. In general, they describe overall vibrational modes of the solid. In the case of molecularly structured nanoparticles, however, the interaction between the constituent molecules is comparatively weak so that the properties of the Lorentz model oscillators should be directly related to the molecular oscillators modulated by the intermolecular interaction. Larger deviations thus indicate strong intermolecular interactions. The comparison of vibrational frequencies and transition probabilities of the isolated molecules with the corresponding Lorentz model parameters thus reveals at least the qualitative effects of the intermolecular hydrogen-bond interactions in the nanoparticles (section 5.3).

Because the gas phase is chemically different from the solid particles, we have to rely on ab initio calculations for the properties of the isolated molecule. To extract parameters from the experimental aerosol spectra, which can be compared with the ab initio prediction of isolated dimeric dihydroxyacetone, the Lorentz model parameters are fitted via eq 3 to the experimental extinction spectra in the mid-infrared region as described in section 3.2. Apart from the parameters that describe the properties of the individual oscillators, namely, resonance frequency ($\tilde{\nu}_s$), reduced oscillator strength (f_s), and damping width (γ_s) (eq 5), two parameters deserve special attention: the offset, ϵ_e, of the dielectric function and the total number of oscillators.

As mentioned in section 3.2, ϵ_e corresponds to the value of the dielectric function at wavenumbers large with respect to the spectral range under consideration but small with respect to electronic excitations—in other words, the overall electronic contribution to the dielectric function.[23] This parameter essentially represents an offset to the real index of refraction. For the very small particle diameters investigated here, the contribution of scattering to the extinction is too small to determine the parameter ϵ_e unambiguously. From eq 6, one finds that $\epsilon_e \approx$

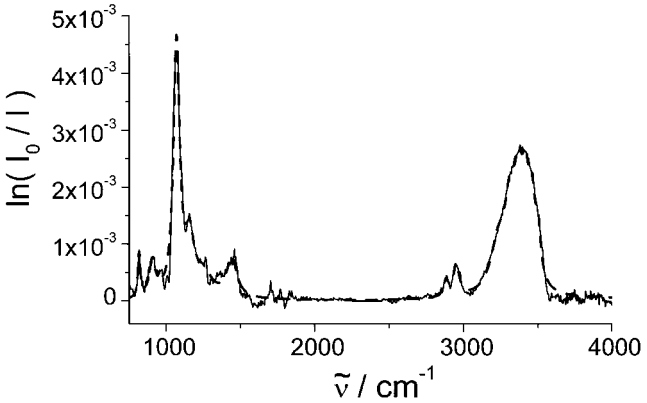

Figure 8. Experimental particle spectrum (full line) as shown in the top trace of Figure 6 and calculated particle spectrum (dashed line) assuming a Kramers−Heisenberg dielectric function (eq 5). The optimized parameters are listed in Table 3.

n_e^2, where n_e is the index of refraction in the visible region of the spectrum (the lowest electronic excitations of dihydroxyacetone lie in the ultraviolet). The value n_e is not known experimentally for amorphous dihydroxyacetone. Instead, we take the typical value of $n = 1.5$ at 589 nm for highly concentrated aqueous sugar solutions.[39] The value of ϵ_e was held fixed at the corresponding value of 2.25.

The number of oscillators included in eq 5 is not determined a priori. In the limit of vanishing interactions between the molecules, it should be given by the number of (IR-active) vibrational modes of the molecule (excluding usually weak combination and overtone transitions). Specific intermolecular interactions (i.e., other than the unspecific damping described by the Lorentz model parameter γ) can produce additional vibrational structure. Two limiting cases may be distinguished: homogeneous structure resulting from the intermolecular coupling (and corresponding splitting) of vibrations (which is the same for all molecules involved in the coupling) and heterogeneous structure resulting from the different environment individual molecules may experience. These two cases cannot be distinguished per se, and both can be described by including additional Lorentz oscillators in eq 5. In principle, any band shape can be simulated with a sufficiently large number of oscillators. Although the number of oscillators is a free parameter of the Lorentz model, it is clear from the above discussion that a physically meaningful parametrization should keep the number of oscillators as small as possible. The number of IR-active oscillators of the isolated molecule can serve as a guideline. Under these conditions, deviations between the properties of the isolated molecule (calculated ab initio) and the experimental Lorentz model parameters can be interpreted in terms of the effects of intermolecular interactions.

As an illustration of the fit, Figure 8 compares an experimental aerosol spectrum (full line) with a calculated particle spectrum (dashed line). The corresponding optimized parameters are listed in Table 3. The dominant features in the extinction spectrum are well-described by the Lorentz model with a small number of oscillators—essentially one for each major absorption band with the notable exception of the OH stretching band at 3400 cm^{-1} (see the discussion in the following section). For the very small particles considered here, scattering contributions are found to be small so that the extinction is largely determined by the imaginary part of the refractive index. The real part of the refractive index is still valuable to judge the quality of the fit: By the nature of the Kramers−Kronig relation (eq 7), nonlocal (on the $\tilde{\nu}$ axis) features of k translate into local features

TABLE 3: Refined Parameters of the Kramers−Heisenberg Dielectric Function in Eq 5[a]

$\tilde{\nu}_s$, cm^{-1}	$f_s \times 10^3$	γ_s, cm^{-1}
3497.1	0.323	42.5
3455.8	0.570	51.0
3413.4	0.784	58.4
3366.5	1.036	70.6
3310.8	1.192	87.8
3232.4	1.183	127.8
2949.2	0.350	48.0
2880.7	0.140	36.2
1440.8	2.894	79.6
1253.4	3.479	130.8
1158.6	5.073	69.3
1067.3	22.576	50.2
957.3	0.354	14.5
905.7	4.634	50.9
816.2	2.592	18.8

[a] The parameter ϵ_e is fixed to the value 2.25.

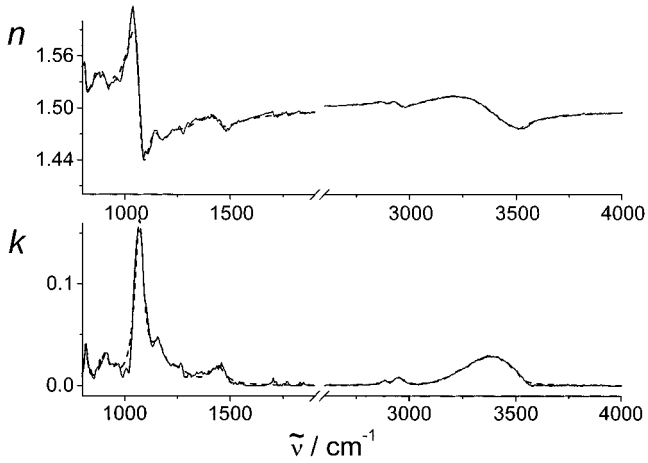

Figure 9. The real part n and the imaginary part k of the complex refractive index (full line) obtained by a Kramers−Kronig inversion of the experimental particle spectrum (eq 7, $n(\tilde{\nu}_r = 2600\ cm^{-1}) = 1.505$ from the Lorentz model) and n and k from a fit of the experimental particle spectrum (dashed line) assuming a Kramers−Heisenberg dielectric function (eqs 5 and 6).

of n and vice versa. Consequently, n is sensitive to those systematic deviations in k that are distributed over the whole frequency range and thus hardly discernible in the extinction trace. Figure 9 compares the complex index of refraction resulting from the Lorentz model (dashed lines) with the corresponding data obtained by direct Kramers−Kronig inversion (full line) of the aerosol spectrum of Figure 8. As expected the traces of the imaginary part of the refractive index mimic the behavior of the extinction spectra. The overall (nonlocal) agreement of n demonstrates that no local features are missing in k as modeled by the set of oscillators listed in Table 3. Small local deviations in n indicate slight imperfections in the representations of band shapes, for example, for the most prominent band at 1080 cm^{-1}. (Here, n is largely determined by the derivative of the k trace.) This could be remedied through the inclusion of further weak oscillators at the loss of the models compactness. The deviations, however, are very small confirming that our present model is not missing any important features.

As discussed in section 3.2, the main origin for the uncertainty of the absolute values of the optical constants comes from the effective optical absorption path length, h. Given the small variations of the real index of refraction, $n(\tilde{\nu})$ (a few percent), the extinction cross section for the small particles under consideration is approximately proportional to k. Therefore, the

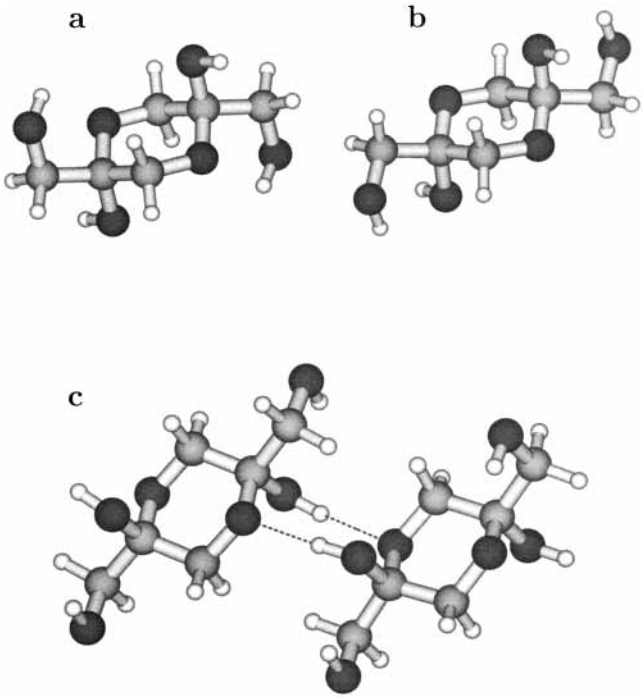

Figure 10. Equilibrium structures of the dimer (a, ee-rr conformer; b, ee-hh conformer) and of the tetramer (c, $(ee)_2$) of dihydroxyacetone. See also text and Table 4. O, C, and H atoms are represented by dark, medium, and light gray spheres, respectively.

uncertainty of h translates into a constant (unknown) scaling factor of $k(\tilde{\nu})$. From eq 7, it follows that this scaling factor is the same for $n(\tilde{\nu}) - n(\tilde{\nu}_r)$. We have confirmed this assumption by calculations assuming an optical path length of 8 m, the estimated lower bound (section 3.2). The resulting values for k double compared with the nominal path length of 16 m. Following the discussion in section 3.2, the (unknown) value of the real scaling factor probably lies closer to 1.0 than to 2.0, the two limiting values.

5.3. Molecular Interactions. As outlined in sections 4 and 5.1, the gas phase in equilibrium with the bulk or particulate matter consists of dihydroxyacetone monomer. For the dimeric form, there are no experimental gas-phase spectra available. Therefore, we have to rely on theoretical predictions for the properties of the molecular constituents of the aerosol particles. Section 4 has established the reliability of the DFT approach chosen for the monomer by careful comparison with higher level theoretical approaches and − most importantly − by comparison with experimental gas-phase spectra. This holds for the spectroscopic properties as well as for the hydrogen-bonding characteristics. We can thus be confident that the same B3LYP/6-31G** approach will also provide a realistic at least semi-quantitative representation of the hydrogen-bonding situation in the dimer, in particular regarding its effects on the spectroscopic properties.

The minimum structure of one of the isomers resulting from the most stable chair conformation of the dioxane ring is depicted in Figure 10a. This isomer has two equatorial CH_2OH groups (labeled ee). The remaining two isomers have one equatorial and one axial CH_2OH group (labeled ea) and two axial CH_2OH groups (labeled aa). Similar to the situation in the monomer, the torsional angles of the OH and CH_2OH groups span a six-dimensional conformational space for each isomer with a correspondingly large number of local minima determined by the intramolecular hydrogen-bonding characteristics. The higher dimensionality precludes a complete dynamical treatment, but by analogy, we can transfer some qualitative conclusions drawn from the 4D dynamics of the monomer. Thus, the separation of time scales between the C−C torsion of the CH_2OH groups and the torsion of the OH groups will lead to an analogous reduction of the number of spectroscopically distinguishable conformations. Indeed, the investigation of the conformational space of the dimer of dihydroxyacetone reveals a simple systematic behavior of the intramolecular hydrogen bonding. The relative stability of different conformers is determined by the C−C torsion of the CH_2OH groups, which can form hydrogen bonds either with the oxygen atom of the dioxane ring (labeled r, Figure 10a) or with that of the hydroxyl groups (labeled h, Figure 10b). Table 4 lists the relative electronic energies, vibrational zero-point energy corrections, and dimerization energies of the most favorable conformers.

TABLE 4: Electronic Energies (E) and Vibrational Zero-Point Energies (ZPE) of Different Isomers and Conformers (see text) of the Chemically Bound Dimer 2,5-dihydroxymethyl-2,5-dihydroxy-1,4-dioxane with Respect to the Most Stable Structure ee-rr[a]

	ΔE (hc cm^{-1})	ΔZPE (hc cm^{-1})	ΔH_0^0 (hc cm^{-1})
ee-rr	0	0	−2430
ee-hh	705	−13	−1738
ea-rr	184	171	−2075
ea-rh	409	44	−1977
aa-rr	891	171	−1368
aa-hh	2448	−207	−189

[a] The electronic energy of the structure ee-rr amounts to −687.188 301 E_h, and its ZPE is 43 399 cm^{-1}. The dimerization energies (ΔH_0^0; including zero-point correction) are given relative to the monomer cccc (see Table 2). The calculations were performed on the B3LYP/6-31G** level.

Figure 11 compares the gas-phase infrared spectra calculated for the most stable rr-conformers of each isomer with an experimental aerosol spectrum. The most prominent difference is the huge shift of the OH-stretching band in the particle spectra by more than 400 cm^{-1} toward lower wavenumbers. It is to be compared with a difference of about 150 cm^{-1} between the harmonic ab initio transition wavenumber and the corresponding band position in the experimental gas-phase spectrum of the monomer (see Figure 2). The large shift of the OH-stretching band in the particle spectrum thus cannot be explained by deficiencies of the calculations such as the neglect of anharmonicities. The reasonable agreement between the theoretical spectra of the isolated molecule and the experimental particle spectrum in the fingerprint region below 1500 cm^{-1} indicates that the molecular integrity of the dimer is retained in the aerosol particles, possibly with the ee-rr conformer as the dominant constituent. The large shift of the OH-stretching fundamental must therefore be due to the environment in the solid phase. The significant broadening as well as the much increased intensity are clear indications of strong intermolecular hydrogen bonds.

The analysis of the nanoparticle spectra in terms of the Lorentz model allows us to compare experimental reduced oscillator strengths (f_s) and resonance wavenumbers ($\tilde{\nu}_s$), eq 5, directly with ab initio predictions for the molecular subunits of the aerosol particles. The stick spectra in Figure 12 illustrate this for the reduced oscillator strengths of the Lorentz model (multiplied by $\tilde{\nu}_s^2$) (panel a) and the fundamental transition intensities calculated ab initio for the most stable conformer of dimeric dihydroxyacetone (panel b). For the fingerprint region, the comparison confirms the good agreement between the intensity distribution in the aerosol spectra and the calculated

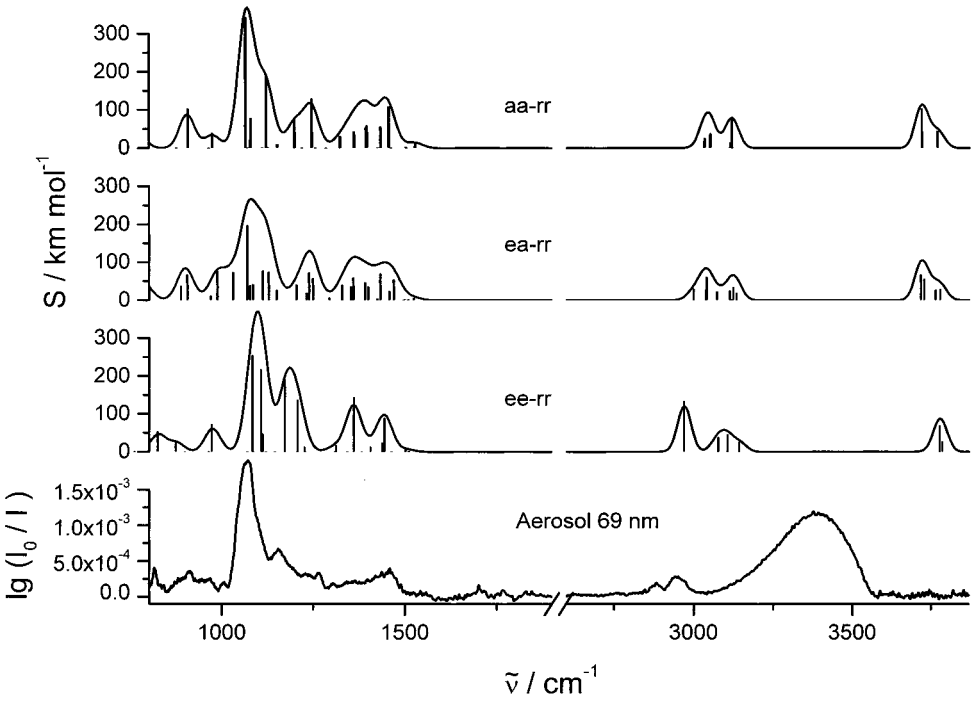

Figure 11. Experimental particle spectrum (bottom trace) as shown in the top trace of Figure 6 and ab initio calculated infrared spectra (upper traces) of isolated 2,5-dihydroxymethyl-2,5-dihydroxy-1,4-dioxane molecules (see Table 4). For better comparison, the theoretical stick spectra were convoluted with Gaussian line shapes of 50 cm^{-1} fwhm.

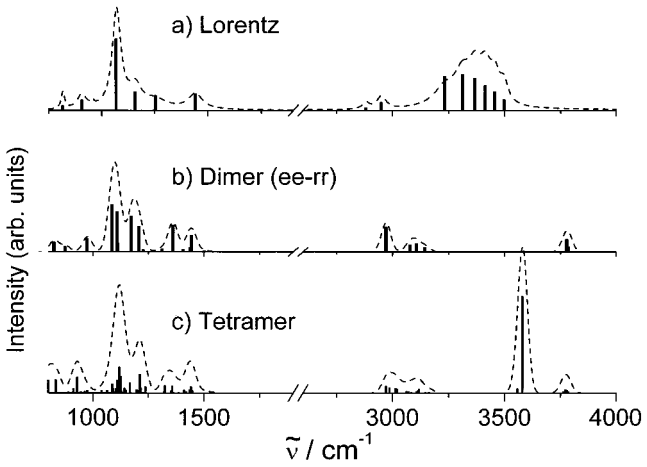

Figure 12. (a) Relative transition intensities, $\tilde{\nu}_s^2 f_s$, for the condensed phase (stick spectrum) of dihydroxyacetone derived from the Kramers−Heisenberg dielectric function (eq 5) and calculated particle spectrum (dashed line) as shown in Figure 8. Panel b shows the transition intensities for dimeric dihydroxyacetone (2,5-dihydroxymethyl-2,5-dihydroxy-1,4-dioxane) from ab initio calculations of the isolated ee-rr isomer. Panel c shows the transition intensities for dihydroxyacetone tetramer (hydrogen-bonded dimer) from ab initio calculations of the isolated molecule. The dashed lines in b and c were obtained by convolution the theoretical stick spectra with a Gaussian line shape of 50 cm^{-1} fwhm.

vibrations of the molecular frame of the isolated molecule. Because of uncertainties in the effective optical absorption path and of the local field corrections discussed in section 3.2, only relative intensities can be compared. In the OH-stretching region above 3000 cm^{-1}, we find important qualitative differences between the calculated spectrum and the Lorentz model. Instead of the two types of stretching vibrations calculated for the isolated molecule, a total of six oscillators is required in the Lorentz model to described the observed band shape. Although the exact number of oscillators is arbitrary to some extent, it clearly exceeds the number of different types of OH groups in the dimer. Moreover, their reduced oscillator strengths increase systematically toward lower wavenumbers as do their widths (γ_s). Note that the latter are representative of the coupling strength to the environment. Together with the large shift to lower wavenumbers noted above, all of these observations are clear indications of the presence of strong intermolecular hydrogen bonds.

We have tested this conclusion by calculating the absorption spectrum of the tetramer of dihydroxyacetone, which consists of two dimers held together by two hydrogen bonds (Figure 10c). The predicted stick spectrum is depicted in Figure 12c. Convoluting the stick spectrum with a Gaussian band shape of 50 cm^{-1} fwhm demonstrates that the hydrogen bonding leaves the intensity in the fingerprint region largely unchanged—if anything, slightly improving the agreement with the experimental spectrum. Above 3000 cm^{-1}, however, one observes a large shift of one OH-stretching transition accompanied by a large increase of the transition intensity. Both confirm our above interpretation of the observed particle spectrum. The strong hydrogen bond leads to a certain degree of short-range order in the amorphous solid state of the aerosol particles. On longer ranges, the hydrogen-bond interaction weakens corresponding to smaller shifts and reduced oscillator strengths relative to the isolated dimer. At the same time, the coupling to the environment becomes weaker, hence, the narrower widths found in the Lorentz model toward higher frequencies.

These results on the amorphous solid particles also offer an explanation for the characteristic band observed near 3200 cm^{-1} in the absorption spectrum of the crystal (Figure 7). It coincides with the low-frequency tail of the particle spectrum. By analogy, we assign it to the antisymmetric stretching vibration of the pairs of OH-groups involved in hydrogen bonds similar to those of the tetramer. The crystal could thus be built from chains of dimeric dihydroxyacetone. Conclusive results, however, can only be obtained from an X-ray structure determination of crystalline dihydroxyacetone.

6. Conclusions

Aerosol spectroscopy provides the link between the spectroscopic investigation of bulk matter and molecular spectroscopy in the gas phase. As the present study has demonstrated, it is particularly well-suited to relate molecular properties to the spectroscopic properties of molecularly structured condensed phases. The prerequisite is an independent characterization of the particulate phase, above all the particle size distribution.

With their multiple hydrogen-bonding valencies, sugars are ideal model systems for the formation of hydrogen-bonded networks in competition with intramolecular hydrogen bonding and rearrangement. The present first study of this kind was conducted on the simplest triose, dihydroxyacetone, still small enough to be accessible to a very detailed theoretical characterization. In the course of the investigation, it turned out to be a perfect example for the interplay between conformational dynamics, aggregation, and chemical rearrangement. The aerosol formed from aqueous solutions in an electrospray was found to consist of two chemically different phases. The first infrared spectrum of dihydroxyacetone vapor in comparison with extensive ab initio calculations shows that the gas phase consists of various hydrogen-bonded and open conformers of 1,3-dihydroxy-2-propanone. The study of the temperature dependence of the spectra in combination with detailed quantum-mechanical models of the conformational dynamics allowed the first quantitative characterization of the multidimensional conformational dynamics. In this prototype system, the effective adiabatic separation of time scales leads to an equilibrium between two spectroscopically distinguishable conformers with an intramolecular hydrogen-bond energy of about 10 kJ/mol.

The analysis of the aerosol spectra leads to the conclusion that the aggregation of dihydroxyacetone molecules in the aerosol particles is accompanied by the formation of intramolecular hemiketals, that is, chemically bound dimers. In contrast to thin layers formed by evaporation of solutions in methanol, the dimerization is complete in the aerosol with no monomer left. The aerosol spectra do not only show that the particles with diameters around 50 nm consist of a solid phase. Over a diameter range of 20 to 90 nm, the particles' optical properties do not change significantly and are qualitatively similar to a theoretical bulk with the same optical constants. This in itself is a by no means trivial result because other molecularly structured systems do show marked size effects in the same diameter range (e.g., CO_2/N_2O[18]). The analysis of the optical properties of dihydroxyacetone nanoparticles in terms of a Lorentz model also allows a direct comparison with molecular properties, which can be calculated ab initio. DFT calculations of small oligomers lead to the conclusion that strong intermolecular hydrogen bonds between chemically bound dimers produce some degree of short-range order in an otherwise amorphous solid. The same hydrogen-bonding mechanism could produce infinite hydrogen-bonded chains of dimeric dihydroxyacetone molecules. Therefore, it could be responsible for the characteristic band structure observed in the OH-stretching fundamental range of the IR spectra of crystalline dihydroxyacetone.

Further insight into the interplay of conformational dynamics, chemical dimerization, and aggregation of this prototype system is to be expected from detailed investigations of the conditions of aerosol formation, in particular the particle growth directly from the vapor. These experiments are currently under way in our laboratory together with complementary studies of the laser-induced melting and crystallization of amorphous nanoparticles. For this type of study, aerosol spectroscopy provides a powerful analytical tool to relate the condensed phase to the properties of its molecular constituents.

Acknowledgment. Support from Prof. M. A. Suhm at the University of Göttingen is gratefully acknowledged. The initial phase of this work was supported by the Deutsche Akademie der Naturforscher Leopoldina through Grant No. BMBF-LPD 9901/8-17 (R.S.). Part of the extensive calculations presented here have been performed within the C4 project at the Department of Chemistry at ETH Zürich.

References and Notes

(1) Quack, M.; Suhm, M. A. In *Spectroscopy and quantum dynamics of hydrogen fluoride clusters*; Bowman, J. M., Bačić, Z., Eds.; JAI Press: Greenwich, U.K., 1998; Vol. III.

(2) Häber, T.; Schmitt, U.; Suhm, M. A. *Phys. Chem. Chem. Phys.* **1999**, *1*, 5573−5582.

(3) Signorell, R.; Kunzmann, M. K.; Suhm, M. A. *Chem. Phys. Lett.* **2000**, *329*, 52−60.

(4) Lozynski, M.; Rusinska-Roszak, D.; Mack, H.-G. *J. Phys. Chem. A* **1997**, *101*, 1542−1548.

(5) Kobayashi, Y.; Ingarashi, T.; Takahashi, H.; Higasi, K. *J. Mol. Struct.* **1976**, *35*, 85−99.

(6) Hinds, W. C. *Aerosol Technology*; Wiley-Interscience: New York, 1999.

(7) Devlin, J. P.; Joyce, C.; Buch, V. *J. Phys. Chem. A* **2000**, *104*, 1974−1977.

(8) Huang, J.; Bartell, L. S. *J. Phys. Chem.* **1995**, *99*, 3924−3931.

(9) Niedziela, R. F.; Norman, M. L.; DeForest, C. L.; Miller, R. E.; Worsnop, D. R. *J. Phys. Chem. A* **1999**, *103*, 8030−8040.

(10) Disselkamp, R. S.; Anthony, S. E.; Prenni, A. J.; Onasch, T. B.; Tolbert, M. A. *J. Phys. Chem.* **1996**, *100*, 9127−9137.

(11) Buck, U.; Krohne, R.; Schütte, S. *J. Chem. Phys.* **1997**, *106*, 109−115.

(12) Dunder, T.; Miller, R. E. *J. Chem. Phys.* **1990**, *93*, 3693−3703.

(13) Fleyfel, F.; Devlin, J. P. *J. Chem. Phys.* **1990**, *92*, 36−42.

(14) Gough, T. E.; Wang, T. *J. Chem. Phys.* **1996**, *105*, 4899−4904.

(15) Disselkamp, R.; Ewing, G. E. *J. Chem. Phys.* **1993**, *99*, 2439−2448.

(16) Bauerecker, S.; Taraschewski, M.; Weitkamp, C.; Cammenga, H. K. *Rev. Sci. Instrum.* **2001**, *72*, 3946.

(17) Häber, T.; Schmitt, U.; Emmeluth, C.; Suhm, M. A. *Faraday Discuss. 118*, **2001**.

(18) Kunzmann, M. K.; Signorell, R.; Taraschewski, M.; Bauerecker, S. *Phys. Chem. Chem. Phys.* **2001**, *3*, 3742−3749.

(19) Milham, M. E.; Frickel, R. H.; Embury, J. F.; Anderson, D. H. *J. Opt. Soc. Am.* **1981**, *71*, 1099−1106.

(20) Clapp, M. L.; Miller, R. E.; Worsnop, D. R. *J. Phys. Chem.* **1995**, *99*, 6317−6326.

(21) Hudgins, D. M.; Sandford, S. A.; Allamandola, L. J.; Tielens, A. G. G. M. *Astrophys. J., Suppl. Ser.* **1993**, *86*, 713−722.

(22) Kuzmany, H. *Solid-State Spectroscopy*; Springer-Verlag: Berlin, 1998.

(23) Bohren, C. F.; Huffman, D. R. *Absorption and Scattering of Light by Small Particles*; Wiley-Interscience: New York, 1998.

(24) Chen, D.-R.; Pui, D. Y. H.; Kaufman, S. L. *J. Aerosol Sci.* **1995**, *26*, 963−977.

(25) Kaufman, S. L.; Caldow, R.; Dorman, F. D.; Irwin, K. D.; Pöcher, A. *J. Aerosol Sci.* **1999**, *30*, S373−S374.

(26) Bauerecker, S.; Taucher, F.; Weitkamp, C.; Michaelis, W.; Cammenga, H. K. *J. Mol. Struct.* **1995**, *348*, 237−241.

(27) Taucher, F.; Weitkamp, C.; Cammenga, H. K.; Bauerecker, S. *Spectrochim. Acta A* **1996**, *52*, 1023−1027.

(28) Frisch, M. J.; Trucks, G. W.; Schlegel, H. B.; Scuseria, G. E.; Robb, M. A.; Cheeseman, J. R.; Zakrzewski, V. G.; Montgomery, J. A., Jr.; Stratmann, R. E.; Burant, J. C.; Dapprich, S.; Millam, J. M.; Daniels, A. D.; Kudin, K. N.; Strain, M. C.; Farkas, O.; Tomasi, J.; Barone, V.; Cossi, M.; Cammi, R.; Mennucci, B.; Pomelli, C.; Adamo, C.; Clifford, S.; Ochterski, J.; Petersson, G. A.; Ayala, P. Y.; Cui, Q.; Morokuma, K.; Malick, D. K.; Rabuck, A. D.; Raghavachari, K.; Foresman, J. B.; Cioslowski, J.; Ortiz, J. V.; Stefanov, B. B.; Liu, G.; Liashenko, A.; Piskorz, P.; Komaromi, I.; Gomperts, R.; Martin, R. L.; Fox, D. J.; Keith, T.; Al-Laham, M. A.; Peng, C. Y.; Nanayakkara, A.; Gonzalez, C.; Challacombe, M.; Gill, P. M. W.; Johnson, B. G.; Chen, W.; Wong, M. W.; Andres, J. L.; Head-Gordon, M.; Replogle, E. S.; Pople, J. A. *Gaussian 98*, revision A.7; Gaussian, Inc.: Pittsburgh, PA, 1998.

(29) Luckhaus, D. *Ber. Bunsen-Ges. Phys. Chem.* **1997**, *101*, 346−355.

(30) Luckhaus, D. *J. Chem. Phys.* **2000**, *113*, 1329−1347.
(31) Bertie, J. E.; Zhang, S. L.; Keefe, C. D. *J. Mol. Struct.* **1994**, *324*, 157−176.
(32) Bachrach, R. Z.; Brown, F. C. *Phys. Rev. B* **1970**, *1*, 818−831.
(33) Ahrenkiel, R. K. *J. Opt. Soc. Am.* **1971**, *61*, 1651−1655.
(34) Hawranek, J. P.; Neelakantan, P.; Young, R. P.; Jones, R. N. *Spectrochim. Acta A* **1976**, *32*, 85−98.
(35) Davis, L. *Bioorg. Chem.* **1973**, *2*, 197−201.
(36) Yaylayan, V. A.; Ismail, A. A.; Mandeville, S. *Carbohydr. Res.* **1993**, *248*, 355−360.
(37) Yaylayan, V. A.; Ismail, A. A. *Carbohydr. Res.* **1995**, *276*, 253−265.
(38) Yaylayan, V. A.; Harty-Majors, S.; Ismail, A. A. *Carbohydr. Res.* **1999**, *318*, 20−25.
(39) Weast, R. C. *CRC Handbook of Chemistry and Physics*; CRC Press: Boca Raton, FL, 1989−1990.